

The insulation structure of the 1 MV transmission line for the ITER neutral beam injector

A. De Lorenzi^{a,*}, L. Grando^a, R. Gobbo^b, G. Pesavento^b,
P. Bettini^c, R. Specogna^c, F. Trevisan^c

^a *Consorzio RFX, Associazione Euratom-Enea sulla Fusione, Corso Stati Uniti 4, I-35127 Padova, Italy*

^b *DIE, Università di Padova, Via Gradenigo 6A, I-35100 Padova, Italy*

^c *DIEGM, Università di Udine, Via delle Scienze 208, I-33100 Udine, Italy*

Received 28 July 2006; received in revised form 12 March 2007; accepted 13 March 2007

Available online 1 May 2007

Abstract

The paper describes the studies and the tests for the development of the insulation structure of the 1 MV–50 A gas insulated (SF₆) line of the ITER NBI in the SinGap configuration characterized by two kinds of spacers: at least a couple of disk-shaped spacers, designed to be gas tight, and a larger number (several tens) of inner conductor post spacers. To this aim a test campaign has been carried out to assess the capability of standard epoxy spacers to withstand a high dc voltage with frequent short circuits, simulating the operational condition for the ITER NBI. Two computational tools, the first for the epoxy spacer shape optimization under electrostatic distribution and the other for the nonlinear time variant evolution of the electric field and surface charge, have been developed specifically for designing epoxy spacer under dc voltage stress. The results on the optimization of the disk spacer and on the electric field–surface charge time evolution of the post spacer are reported and discussed. The effects of the SF₆ radiation induced conductivity on the post spacer are also reported.

© 2007 Elsevier B.V. All rights reserved.

Keywords: Neutral beam injector (NBI); HVDC; Epoxy–SF₆; Electric field transition; Charge accumulation; Radiation induced conductivity (RIC)

1. Introduction

For the neutral beam injector (NBI) single gap configuration [1], the power supply system feeds the beam

source through a SF₆ gas insulated coaxial conductor (transmission line, TL) with the inner electrode polarized at the negative potential of 1 MV dc [2]. TL then belongs to the gas insulated line (GIL) family, whose technology is nowadays mature for ac applications up to 1000 kV rms, but not yet for HVDC. In fact, the spacers design (post and disk epoxy resin insulators) for HVDC with the same degree of reliability already

* Corresponding author. Tel.: +39 049 829 5016; fax: +39 049 870 0718.

E-mail address: antonio.delorenzi@igi.cnr.it (A. De Lorenzi).

available for HVAC is far away from being attained, due to the substantial difference between ac (capacitive) and dc (resistive) voltage electric field distribution and insulation behavior at epoxy–SF₆ interface. Furthermore, the particular NBI voltage waveform (dc constant voltage applied for 1 h during which very frequent short circuits will occur [1]) introduces additional elements of uncertainty in the design of the insulation structure, due to the difficulty to evaluate the time constant of the resistive electric field distribution set-up.

The other key issue for the TL insulation design is the presence of the residual metal particles inside the tank, very harmful to the insulation stability. The management of such aspect and the related solutions (electrode coating, electrostatic traps, voltage conditioning, etc. [3]) are nevertheless similar to HVAC practice and it will be not treated here.

Finally, part of the ITER NBI transmission line will be installed inside a radioactive environment, which modifies the conductivity of the insulating media.

This paper aims at giving an effective design strategy to take into account the peculiar operating conditions of the TL and related equipments; to accomplish this task, the following activities have been carried out.

First, an experimental campaign has been undertaken aimed to assess the compatibility, not proven by any industrial experience, of epoxy resin insulator and SF₆ to voltage waveform like those occurring in NBI operation. These tests have been performed on a scaled model of TL, where the electric field is similar to that which can reasonably be envisaged for the full scale TL.

Second, a nonlinear-time variant code has been developed in ANSYSTM environment, to evaluate the electric field and charge time evolution in the spacer, considering the nonlinear surface conductivity of the epoxy resin [4].

Third, a spacer optimization tool has been developed based on a discrete geometric approach [5], to find the “best” spacer shape and screen profile of the triple point (the intersection among gas, solid insulator and electrode).

These computational methods have then been used for the preliminary design of the post and disk spacer, with the aim to minimize the surface charge density during the evolution of the electric field: such criteria, in fact, have been proven [7] to be effective in increasing the long term voltage stability of epoxy–SF₆ interface.

To minimize the transmission line volume for a given value of the internal conductor electric field, the inner and outer diameters shall be in the ratio:

$$\frac{D_e}{D_i} = e = 2.718 \dots \quad (1)$$

The internal conductor electric field has been set to 5 kV/mm at 1 MV with a SF₆ pressure of 0.3 MPa; the safety factor respect to the SF₆ theoretical breakdown electric field (89 kV/(mm MPa)) is about 5, similar to that used in industrial applications; being $E_i = 2(V/D_i)$ the electric field at the inner conductor, the TL internal and external diameters will be 400 and 1100 mm, respectively.

2. Experimental campaign

The component under test is a disk-shaped spacer used for gas insulated switchgear with the following voltage ratings:

$U_n = 170 \text{ kV}_{\text{rms}}$	Rated rms voltage
$U_W = 325 \text{ kV}_{\text{rms}}$	1 min power frequency rms withstand voltage
$U_{LI} = 750 \text{ kV}_{\text{peak}}$	1.2/50 μs standard lightning impulse withstand voltage

This insulator is made of a mixture of bisphenolic epoxy resin + reactants and alumina (Al₂O₃) with ratios of 40% and 60% (in weight), respectively. Three spacers have been employed in the same assembly, as shown in Fig. 1. The SF₆ pressure has been chosen 0.3 MPa absolute.

A –200 kV dc voltage with a negligible ripple was applied; the electric field distribution has been evaluated by computation, considering three possible conditions: pure capacitive, pure resistive with uniform conductivities γ_{epoxy} , γ_{SF_6} and – the most likely – pure resistive with nonzero surface conductivity γ_s of the spacer. Fig. 2 shows the field components – E_t tangential and E_n normal to the spacer surfaces – for the initial capacitive distribution and the final distribution in case of nonzero surface conductivity. Surface conductivity γ_s has actually a nonlinear dependence with the tangential electric field E_t and temperature [4]:

$$\gamma_s = \gamma_{0s} e^{\alpha E + \beta T}, \quad (2)$$

$\gamma_{0s} = 10^{-19}$ to 10^{-20} (S), $\alpha = 1.25$ – 1.3 (mm/kV) and $\beta = 0.05$ (1/K).

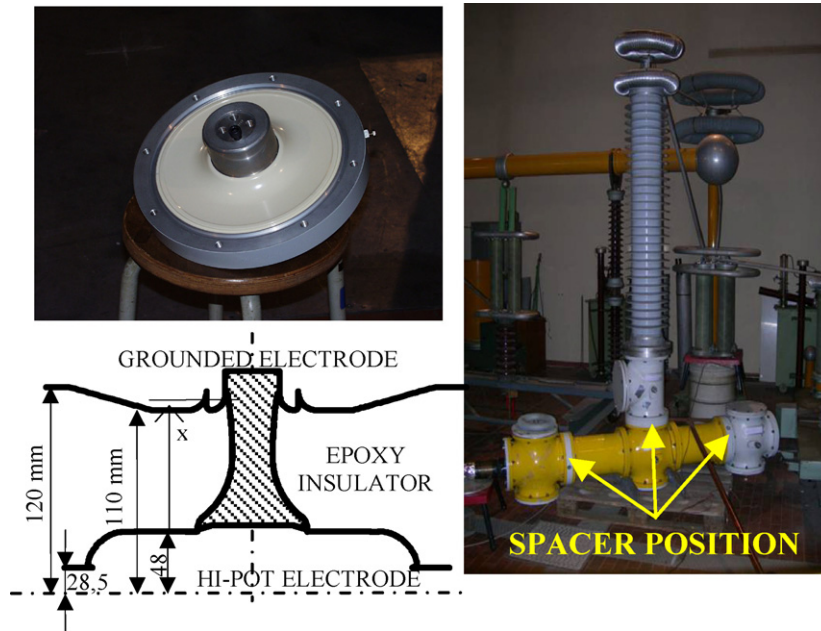


Fig. 1. Spacer and test assembly.

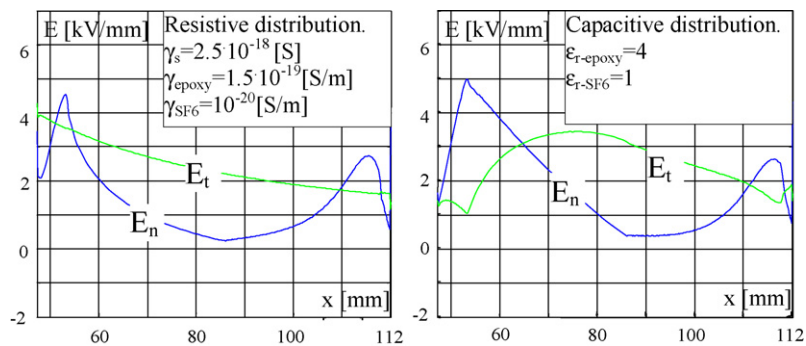


Fig. 2. Tangential and normal field along the spacer surface.

The γ_s value indicated has been evaluated assuming an average field of 2.5 kV/mm and neglecting the temperature dependence; however such a simplification does not affect greatly the final resistive electric field distribution. In all the conditions the computed tangential and normal electric fields are close to the limit of 5 kV/mm. The test assembly has been subjected to the test sequence indicated in Table 1.

Fig. 3 shows the scheme of the circuit used to produce the required test sequence. The circuit on the left side consists of a voltage doubler applying -200 kV to

Table 1
Test sequence applied to epoxy spacers

Voltage applied (0.1% ripple)	200 kV _{dc}
Number of short circuits	1500
Repetition rate	1/15 min
Voltage re-application time	0.4 s
Total voltage application time	375 h
Daily	8 h over 24 h
Weekly	5 over 7 days
Total weeks	9
Consecutive weeks	5

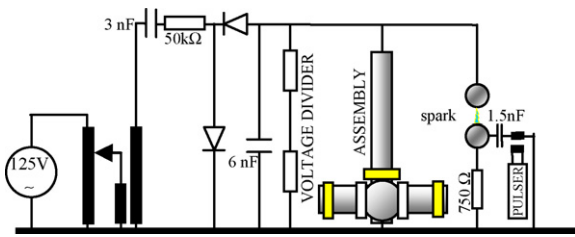


Fig. 3. Scheme of the circuit for testing the spacers.

the assembly; every 15 min the spark-gap is triggered, producing a voltage collapse with 5.5 μs time constant. A circuit model has been then derived and validated by current measurement.

The occurrence of possible ionization phenomena inside the tank has been monitored by means of a photomultiplier on the view line of one spacer. A photon counting head has also been used for increased sensitivity.

Fig. 4 shows the voltage pattern during chopping: a high frequency oscillation – due to ringing of the 1.5 nF capacitor with the stray inductances – is superimposed to the RC decay. The estimated oscillation amplitude seems insufficient to produce voltage reversal, so that any information cannot be derived for such highly stressing condition [3] which in case of transmission line internal breakdown, is very likely.

As far the capacitive to resistive distribution characteristic time is concerned, it can be evaluated using the following approximate formula [7]:

$$T(h) = \frac{\epsilon_{SF6} + \epsilon_{epoxy}}{\gamma_{SF6} + \gamma_{epoxy} + (\gamma_s/R_0)} = 490 \quad (3)$$

where the parameters are those indicated in Fig. 2 and R_0 is the characteristic dimension (radius) of the spacer

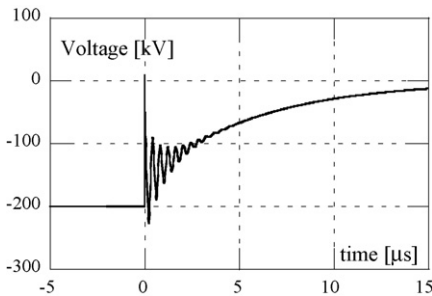


Fig. 4. Voltage waveform applied to the assembly.

(~0.1 m). The actual time constant T could be nevertheless lower by one or even two order of magnitudes, due to the uncertainty in the determination of γ_s .

In any case, when considering the test sequence summarized in Table 1, it can be concluded that fully resistive distribution likely was not reached during the test; the actual electric field distribution would be then an intermediate distribution between pure capacitive and pure – superficial – resistive.

After the tests the spacers have been subjected to accurate surface inspection, X-ray analysis and microscope 400× analysis of a spacer section. No evidence of partial discharge or surface tracking has been found. During the tests, the photomultiplier and photon counting device did not detect any light pulse emission, so that it can be argued that conductivity modifications of SF₆ due to ionization phenomena did not occur.

These positive test results indicate that the SF₆–epoxy spacer insulating structure is compatible with the operating conditions of the neutral beam transmission line. Nevertheless, these results extrapolation to the 1 MV transmission line insulating structure cannot be done without applying voltage for time longer than 3T–4T.

In addition, experimental evaluation of spacer bulk and nonlinear surface conductivity is also important for the calculation of the electric field time evolution, as described in the following paragraph.

3. Nonlinear-time dependent model

In HVDC regime the current distribution in the epoxy spacers installed in compressed SF₆ gas seems to be governed by the superficial conductivity varying according to the Eq. (2). After the voltage application, the electric field evolves from the capacitive distribution ($t=0$) to the resistive ($t=\infty$) through nonlinear evolution of the surface conductivity. A nonlinear transient procedure has been developed in ANSYSTM environment, implementing an iterative technique which takes into account the modification of the surface conductivity accordingly to Eq. (2) (temperature dependence is neglected).

Such technique consists of the following phases. The nonlinear material property is defined by a $\gamma_s^*(E_t)$ curve, where the superficial conductivity γ_s is transformed into bulk conductivity γ_s^* by means of the

following equation:

$$\gamma_s^* = \frac{\gamma_{0s} e^{\alpha E_t}}{\Delta} \quad (4)$$

being Δ the layer with a limited thickness (typically $\Delta = 100 \mu\text{m}$) to make negligible the voltage drop across its internal boundary. For each k th time step Δt , the ANSYS solver finds the electric field distribution solving the equation $\nabla^2 V = -\rho/\epsilon$, where the charge density ρ is accumulated by the divergence of the current density $\nabla \cdot j = -\partial\rho/\partial t$; the electric field distribution on the spacer surface then evolves following equation:

$$E_k = E_{k-1} + \frac{\gamma(E_{t,k-1})}{\epsilon} E_{k-1} \Delta t \quad (5)$$

where the nonlinear conductivity is taken into account.

4. Disk spacer optimization

Most recent investigations [6,7] found that the steady state charge density accumulated on the spacer surfaces under dc voltage is driven by the normal component E_n and by the spatial gradient ∇E_t of the tangential component E_t of the electric field at the beginning of the process, i.e. with electrostatic distribution. On this condition, a 2D optimization tool can be effectively employed to find the spacer shaping that minimizes E_n and ∇E_t . The optimization tool which has been adopted – in this first stage intended only to minimize E_n and E_t in the disk spacer of Fig. 5 – is hereinafter described.

A direct search optimization method [9] has been used to solve the nonlinear problem (NLP) of minimizing a chosen objective function $f(x)$ under a given number of constraints on design variables x (e.g. geometric parameters like screen curvature radii and spatial coordinates). The objective function $f(x)$ has the form:

$$f(x) = k_1 f_1(x) + k_2 f_2(x) \quad k_1 + k_2 = 1 \quad (6)$$

and both f_1 and f_2 are normalized functions (between 0 and 1) of the electric field components calculated in points laying on the two spacer surfaces.

A new mesh M is generated at each iteration, starting from the actual values of x following this procedure: two cell complexes (M_1 and M_2) are introduced, one (primal complex) is made of triangles, and the other

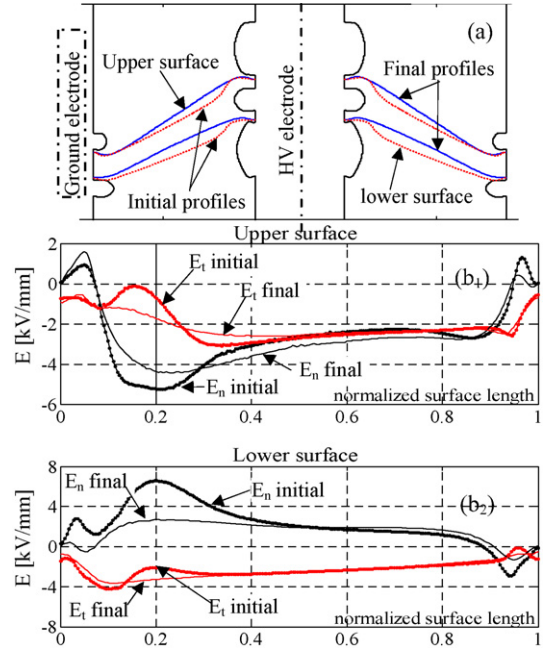


Fig. 5. (a) Disk spacer profile optimization. (b₁ and b₂) Electric fields improvement.

(dual complex) is obtained by connecting the triangles barycentres [10]. In this way the degrees of freedoms (DoFs) array (the unknowns array) is obtained: voltage U (associated to the edges of the M_1), electric flux Ψ (associated with the faces of M_2), electric charges Q (associated with the volumes of M_2). The electrostatic problem can then be cast in a discrete way as follows:

$$-\tilde{D}\epsilon GV = Q \quad (7)$$

where V is the array of the electric scalar potentials such that $U = -GV$; G and \tilde{D} are the incidence matrices defining interconnections between the mesh cells, and ϵ is a square matrix dependent on mesh and media properties which links the DoF arrays Ψ and U . The boundary conditions are assigned in terms of V on the internal conductor and external screen nodes.

Fig. 5 shows the spacer optimization results. It can be seen that the optimization tool reduces E_t below 3.5 kV/mm and E_n below 4.5 kV/mm. The curve is strongly smoothed, thus resulting also in a reduction of ∇E_t . In this optimization the triple point screens shapes have been kept fixed.

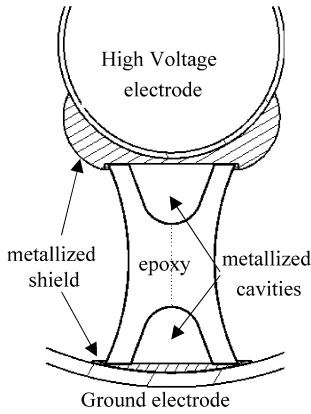


Fig. 6. Post spacer shape.

5. Post spacer nonlinear and time variant analysis

On the post spacer shown in Fig. 6 – whose shape is derived from Ref. [6] and adapted to the cylindrical

geometry of the transmission line – have been carried out first the transient analysis with $\gamma_{\text{epoxy}} \gg \gamma_{\text{SF6}}$ and nonlinear spacer surface conductivity and second the linear steady state analysis with $\gamma_{\text{epoxy}} \ll \gamma_{\text{SF6}}$; this assumption accounts for the effect of SF₆ radiation induced conductivity (RIC) reported in Refs. [11–13]; the ionizing radiation ($\gamma - x$) is produced by scattered neutrons coming from fusion reactions.

The geometry of the post spacer used in the analyses shown in Fig. 6 minimizes the electric surface charge once the fully resistive distribution has been reached. Surface nonlinear conductivity has been modeled by Eq. (4) using $\Delta = 120 \mu\text{m}$.

5.1. Nonlinear transient analysis

Fig. 7a shows as the tangential component of electric field along the spacer surface is being reduced in the middle part of the spacer when passing from a capacitive distribution (6 kV/mm) to a resistive steady state distribution (3 kV/mm) due to the nonlinearity of the

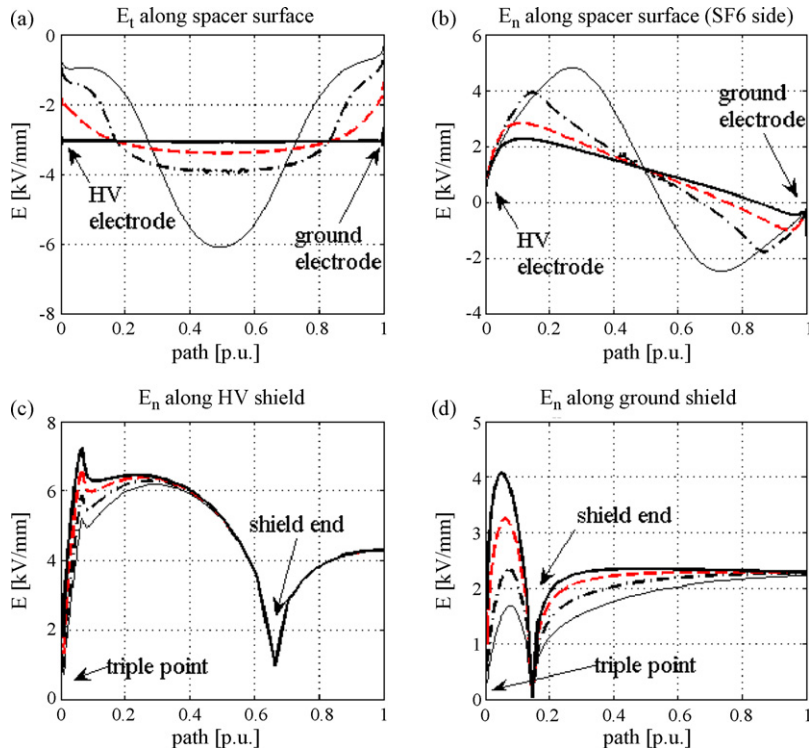


Fig. 7. Time evolution of the electric field along the spacer. Resistive regime reached after 170 h (thin-solid $t=0$; dashed-dot $t=10$ h; dashed $t=50$ h; bold-solid $t=167$ h), $\gamma_s(E_t) = 10^{-19} \exp(1.3E_t)$ (S); $\gamma_{\text{epoxy}} = 10^{-19}$ (S/m), $\gamma_{\text{SF6}} = 10^{-19}$ (S/m), $\epsilon_{r\text{-SF6}} = 1$, $\epsilon_{r\text{-epoxy}} = 4$.

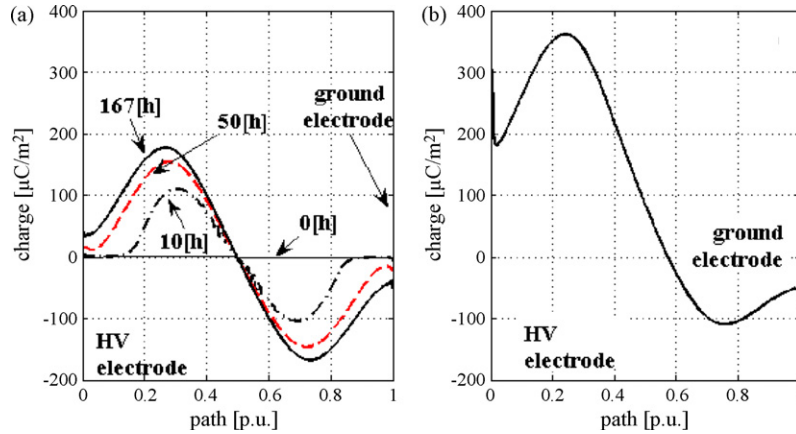


Fig. 8. Time evolution of the charge accumulation along spacer surface. (a) Normal case and (b) RIC.

layer conductivity which reduces the electric gradient. It is important to note that the triple point field necessarily increases under the same conditions due to the fact that E_t is determined by the spacer superficial current density which is much higher than that flowing in the bulk due to the higher surface conductivity. The normal component at SF₆ side (Fig. 7b) decreases too, in consequence of the hetero-charge accumulation on the spacer surface (Fig. 8a). Under the assumptions used for the simulations the surface charge reaches a density of 170 $\mu\text{C}/\text{m}^2$. Such charge distribution would not affect the voltage stability, also in case of superimposed voltage transient provided the voltage does not exhibit reversal [8]. The time constant evaluated by (3), assuming $R_0 = 0.5$ m and $E_t = 4.5$ kV/mm is about 180 h, in good agreement with the simulation results. Fig. 7c and d reports the electric field distribution along the shields surfaces. During the transition between capacitive and resistive distribution there is an enhancement of the field at ledges, from 5 to 7 kV/mm at HV side and from 2.6 to 4 kV/mm at ground side. The minimum of the field located at the intersection between ground electrode and shields might act as an electrostatic trap [4].

5.2. Effect of the radiation induced conductivity of SF₆ on the electric field distribution

The RIC issue is relevant to the transmission line section inside the Tokamak building, where a ioniz-

ing radiation dose rate is expected up to some Gy/s. Experiments and models [11,12] reveal an increase of leakage current per unit volume, depending on dose rate, pressure and independent on voltage applied, provided $E/p > 0.1$ kV/(mm bar):

$$I \text{ (mA)} \approx 50 d_{(\text{Gy/s})} v_{(\text{m}^3)} p_{(\text{bar})} \quad (8)$$

The equivalent conductivity of SF₆ can be derived from (8), at least as an order of magnitude, considering an inter-electrode volume $v = SL$ subjected to $V = 1$ MV across the gap L :

$$\gamma_{\text{SF}_6} \text{ (S/m)} = \frac{L}{S} \frac{I}{V} = 5 \times 10^{-8} p d L^2 = 2.5 \times 10^{-10} \quad (9)$$

being $L = 0.35$ m, $p = 4$ bar and $d = 0.01$ Gy/s (a relatively low value dose). This value, even if uncertain, is many orders of magnitudes larger than bulk and superficial conductivity of the spacer. As a first consequence, the time constant T is greatly reduced so that in few seconds the resistive distribution takes place; spacer surface nonlinearity disappears, masked by the SF₆ conductivity. In this condition (see. Fig. 9), E_t is strongly increased up to 10 kV/mm near to the triple point; E_n inside epoxy spacer increases to 10 kV/mm too, even if this is less dangerous for the insulation stability; the electric field at HV electrode shield is also increased up to 11.5 kV. Hetero-charges density is increased by a factor 2 with respect to normal case (see

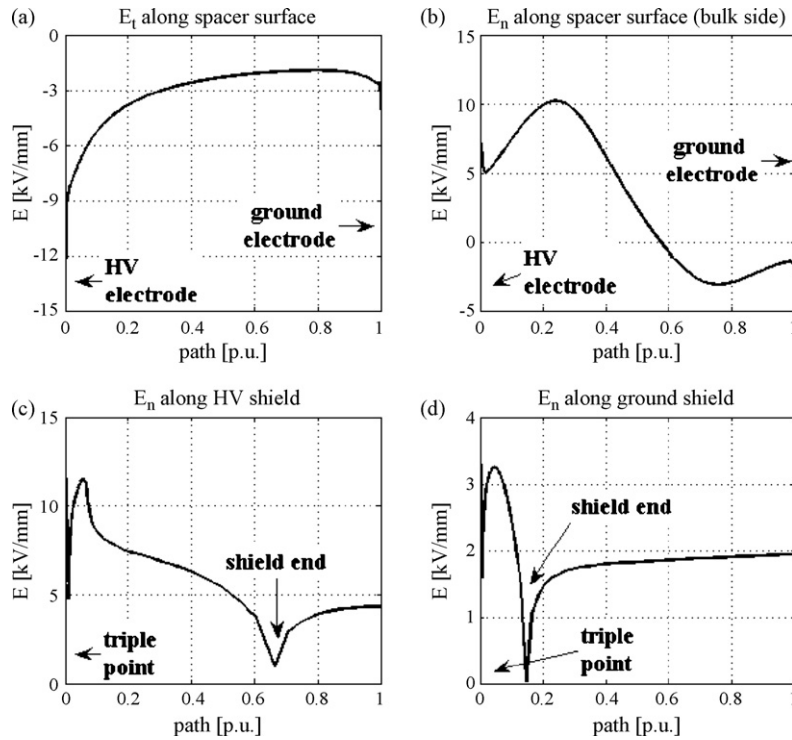


Fig. 9. Resistive electric field distribution along the spacer for the RIC case. $\gamma_{\text{epoxy}} = 10^{-19}$ (S/m), $\gamma_{\text{SF6}} = 2.5 \times 10^{-10}$ (S/m), $\epsilon_{\text{r-SF6}} = 1$ and $\epsilon_{\text{r-epoxy}} = 4$.

Fig. 8b). Under these conditions the insulator failure is very likely.

6. Conclusions

The tests made on a reduced scale showed that choice of the SF₆–epoxy spacer technology is a viable solution for the NBI transmission line insulating structure; nevertheless more comprehensive design approach must be adopted to take into account dc voltage specificity, like surface charge accumulation driven by bulk and nonlinear surface conductivity. For this purpose, a spacer shape optimizer and a ANSYS™ based nonlinear, time-variant code have been developed and applied, respectively, to the disk and post spacer. From tests and computations, the need of a better knowledge of the epoxy bulk and surface nonlinear conductivity emerged, this latter being responsible for the electric field and surface charge temporal evolution. The severe effect of the SF₆ radiation induced conduc-

tivity on insulation withstand capability has been also highlighted.

Acknowledgments

This work, supported by the European Communities under the contract of Association between EURATOM/ENEA, was carried out within the framework of the European Fusion Development Agreement. The views and opinions expressed herein do not necessarily reflect those of the European Commission.

References

- [1] V. Antoni, The ITER Neutral Beam System: Status of the Project and Review of the Main Technological Issues, This Conference.
- [2] K. Watanabe, M. Kashiwagi, S. Kawashima, Y. Ono, Y. Yamashita, C. Yamazaki, et al., Development of a dc 1 MV power supply technology for NB injectors, Nucl. Fusion 46 (2006) S332–S339.

- [3] T. Hasegawa, K. Yamaji, M. Hatano, Development of insulation structure and enhancement of insulation reliability of 500 kV dc GIS, *IEEE Trans. Power Deliv.* 12 (1) (1997) 194–201.
- [4] B.M. Weedy, DC conductivity of Voltalit epoxy spacers in SF₆, *IEE Proc.* 132 (Pt. A) (1985) 450–454, no. 7.
- [5] P. Bettini, F. Trevisan, Electrostatic analysis for plane problems with finite formulation, *IEEE Trans. Mag.* 39 (3) (2003) 1127–1130.
- [6] E. Volpov, Dielectric strength coordination and generalized spacer design rules for HVAC/DC SF₆ gas insulated systems, *IEEE Trans. Dielectr. Electr. Insul.* 11 (6) (2004) 949–963.
- [7] E. Volpov, HVDC gas insulated apparatus: electric field specificity and insulation design concept, *IEEE Electr. Insul. Mag.* 18 (2) (2002) 7–14.
- [8] H. Fujinami, T. Takuma, M. Yashima, T. Kawamoto, Mechanism and effect of DC charge accumulation on SF₆ gas insulated spacers, *IEEE Trans. Power Deliv.* 4 (3) (1989) 1765–1772.
- [9] M.J.D. Powell, Direct search algorithms for optimization calculations, *Acta Numerica* 7 (1998) 287–336.
- [10] E. Tonti, Algebraic topology and computational electromagnetism, in: *Proceedings of the 4th International Workshop on Electric and Magnetic Fields*, Marseille (Fr), May 12–15, 1988, pp. 284–294.
- [11] E.R. Hodgson, A. Moroño, A model for radiation induced conductivity in neutral beam injector insulator gases, *J. Nucl. Mater.* (2002) 307–311.
- [12] E.R. Hodgson, A. Moroño, Radiation effects on insulating gases for the ITER NBI system, *J. Nucl. Mater.* (1998) 258–263.
- [13] Y. Fujiwara, M. Hanada, T. Inoue, K. Miyamoto, N. Miyamoto, Y. Ohara, et al., Radiation induced conductivity and voltage holding characteristics of insulation gas for the ITER NBI, *AIP Conf. Proc.* 439 (1998) 205.